Higher alcohol synthesis over a K-promoted $Co_2O_3/CuO/ZnO/Al_2O_3$ catalyst

Ismail Boz *

Istanbul University, Faculty of Engineering, Department of Chemical Engineering, Avcilar, 34850, Istanbul, Turkey

Received 28 October 2002; accepted 10 February 2003

Higher alcohol synthesis over a K_2O-promoted $Co_2O_3/CuO/ZnO/Al_2O_3$ catalyst has been studied in an internal recycle reactor under steady-state conditions using hydrogen to carbon monoxide inlet ratios between 0.5 and 3.3 and inlet carbon dioxide concentrations between 0 and 10%. The selectivity of hydrocarbons and alcohols with 1–8 carbon atoms was obtained as a function of exit carbon dioxide content, exit hydrogen to carbon monoxide ratio, and operating temperature (498–578 K), using space velocities between 1500 and 15 000 h^{-1} (STP). These experiments, combined with information obtained from active catalyst characterization using XPS, indicated that the chain growth probability factor of higher alcohols was independent of conversion, whereas that of hydrocarbons was dependent on conversion.

KEY WORDS: higher alcohol synthesis; copper/cobalt catalyst; catalyst characterization.

1. Introduction

Considerable effort has been made to understand the mechanism of higher alcohol synthesis and to develop a higher alcohol synthesis catalyst as selective as the Cu-based methanol synthesis catalyst. Recent review articles [1–3] discussed the mechanism and kinetics of higher alcohol synthesis over various catalysts. Catalysts for higher alcohol synthesis fall into one of three broad categories: firstly those producing predominantly branched alcohols, *i.e.* isobutanol, such as K-promoted $Cu/ZnO/Al_2O_3$ catalysts [4–6], secondly those producing predominantly C_{2+} oxygenates, *i.e.* ethanol, such as Rh-based catalysts [1,7,8], and finally those producing predominantly a range of straight-chain alcohols. Straight-chain alcohols are produced over both molybdenum sulfide [1] type catalysts and modified Fischer–Tropsch catalysts, such as Co/Cu-based catalysts [3,9–11].

It was reported by IFP that the products followed a Schulz–Flory-type distribution [10]. Xiaoding *et al.* [1] reported that, under steady-state operating conditions, the chain growth probability factor α of hydrocarbons is equal to that of alcohols and higher CO partial pressures favor higher alcohols. Xiaoding *et al.* [1] also reported that a homogeneous distribution of catalytic sites is a prerequisite for the synthesis of alcohols. C–C chain formation involves CH_x species, originating from metallic Co sites along with the insertion of CO for alcohol production.

Blanchard and co-workers [12] postulated that formation of hydrogenated intermediates took place on metallic sites while CO insertion occurred on oxidized sites. According to their scheme, the production of alcohols on cobalt catalysts can only occur if an intimate contact is achieved between metallic cobalt and copper-modified cobalt oxide.

In this study, higher alcohol synthesis was studied on a 5% K_2O-promoted $Co_2O_3/CuO/ZnO/Al_2O_3$ catalyst. The tests were performed in an internal recycle reactor [13] under well-defined gas-phase conditions. The effects of exit CO_2 concentration, CO conversion, and temperature were investigated. The results were augmented by the characterization of selected catalysts by EDX, BET, and *in situ* XPS. In the characterization studies emphasis was given to the start-up period before the catalyst reached steady-state conditions. Steady-state surface composition and changes in composition were explained within a tentative scheme.

2. Experimental

2.1. Catalyst preparation and activation

The preparation of the catalysts involved the co-precipitation from two aqueous solutions, one of which contained dilute metal nitrates and the other contained sodium carbonate solution. The coprecipitates were left to age in the mother liquor for 1 h at 343 K, dried at 393 K for 19 h, and finally calcined under flowing air at 723 K for 4 h before pelletization into 1/8-inch pellets [14]. Graphite (2% (w/w)) was added as a pilling agent. The pelletized catalysts before calcination were impregnated with different amounts of K_2CO_3, namely 1, 5, and 10% (w/w) as K_2O. Prior to kinetic tests and surface

* To whom correspondence should be addressed.
E-mail: ismailb@istanbul.edu.tr

1011-372X/03/0400-0187/0

Table 1
Catalyst compositions determined by EDX and surface areas

	Composition (wt%) as in oxides	
	Unpromoted Co_2O_3/CuO/ZnO/Al_2O_3 catalyst	5% K_2O-promoted Co_2O_3/CuO/ZnO/Al_2O_3 catalyst
CuO	17.2	16.8
Co_2O_3	13.2	12.6
ZnO	26.3	24.3
Al_2O_3	43.2	41.3
K_2O	–	4.9
BET surface area of fresh catalyst ($m^2\ g^{-1}$)	78	76
BET surface area of used catalyst ($m^2\ g^{-1}$)	59	45

characterization the catalysts were activated with 4.96% (v/v) H_2 in nitrogen at 523 K and 0.5 MPa for 12 h.

The bulk compositions of catalysts were determined using a JEOL 35 EDX spectrometer. Analyses for Co, Cu, Zn, Al, and K were performed and compositions calculated for their common oxides, Co_2O_3, CuO, ZnO, Al_2O_3, and K_2O. Surface area measurements from the BET method and EDX measurements for bulk composition are shown in table 1.

2.2. X-ray photoelectron spectroscopy (XPS)

X-ray photoelectron spectroscopy (XPS) was carried out on the precursor, calcined, reduced catalyst, and after 16 h under simulated reaction conditions over a 5% K_2O-promoted Co_2O_3/CuO/ZnO/Al_2O_3 catalyst. XPS measurements were carried out using a Vacuum Generators ESCALAB Mk II spectrometer. All the treatments were carried out in a reaction cell attached to the XPS apparatus using the exact reduction and reaction gases and temperatures but the pressure was around 2 atm. After the treatments in the attached reactor, the samples were cooled under oxygen-free ultrapure helium and without exposure to air. They were transferred to the XPS unit via vacuum chambers and then XPS measurements were taken. This procedure was repeated after each step of activation, reaction, etc.

AlKα (1486 eV, FWHM 0.83 eV) was used for the X-ray radiation. The X-ray source was operated at 10 kV and 20 mA emission. The energy analyzer was operated in the constant-analyzer mode with pass energy of 50 eV. XP spectra were referenced to the Zn $2p_{3/2}$ peak [15] at 1022.2 eV; the stability of ZnO for this purpose was demonstrated by Moretti *et al.* [16] and also evidenced by the stability of the Zn Auger parameter. Surface compositions were determined as the ratio of intensities based on peak areas (I), taking unity as the relative atomic sensitivity factor for cobalt and 0.88 for copper [16]:

$$\mathrm{Cu/Zn} = I_{(\mathrm{Cu}\,2p_{3/2})}/I_{(\mathrm{Zn}\,2p_{3/2})} \times 1/0.88$$

$$\mathrm{Co/Zn} = I_{(\mathrm{Co}\,2p_{3/2})}/I_{(\mathrm{Zn}\,2p_{3/2})} \times 1/1.$$

Table 2
The changes in copper Auger parameters after various treatments over a 5% K_2O-promoted Co_2O_3/CuO/ZnO/Al_2O_3 catalyst

Catalyst treatment	Auger parameter as $\beta + h\nu$ (eV)
Precursor	1850.57
After 2 h reduction	1848.45
After 4 h reaction	1849.07
After 10 h reaction	1848.81
After 19 h reaction	1848.55

Cu oxidation states were distinguished in the following manner. Cu^{2+} has a peak binding energy of 932.5 eV for Cu $2p_{3/2}$, whereas the binding energies of Cu^0 and Cu^{1+} coincide at 932.2 eV for Cu $2p_{3/2}$. A similar binding energy shift is apparent for Cu $2p_{1/2}$. In the case of Cu^{2+}, the Cu $2p_{3/2}$ peak has a characteristic satellite at approximately 940.0 eV. A Cu $2p_{1/2}$ satellite peak is also characteristic of Cu^{2+}. Cu^{1+} and Cu^0 can be distinguished by calculation of the Auger parameter β, calculated by subtraction of the kinetic energies of the Cu $2p_{3/2}$ photoelectron line and $Cu_{L3M4,5M4,5}$ Auger transition as shown in table 2:

$$\beta = \mathrm{KE}_{2p_{3/2}} - \mathrm{KE}_{\mathrm{L3M4,5M4,5}}$$

According to Moretti *et al.* [16] the addition of the energy of excitation of the source $h\nu$ gives $\beta + h\nu$ values of 1849.4 ± 0.4 eV for Cu^{1+}, compared to 1851.2 ± 0.4 eV for Cu^0 and Cu^{2+}. Changes in the surface compositions are given in table 3. Decreases in the copper and cobalt surface concentrations were, respectively, 83 and 86% relative to precursors.

Table 3
The changes in surface composition determined using the ratios of peak areas over a 5% K_2O-promoted Co_2O_3/CuO/ZnO/Al_2O_3 catalyst

	Precursor untreated	After 2 h reduction	After 4 h reaction	After 10 h reaction	After 19 h reaction
$Cu_{2p_{3/2}}/ZN_{2p_{3/2}}$	3.25	2.93	0.73	1.02	0.55
(loss area %)	(0)	(9.85)	(77.54)	(68.62)	(83.08)
$Co_{2p_{1/2}}/ZN_{2p_{3/2}}$	2.86	2.59	0.78	0.93	0.39
(loss area %)	(0)	(9.44)	(72.73)	(67.48)	(86.36)

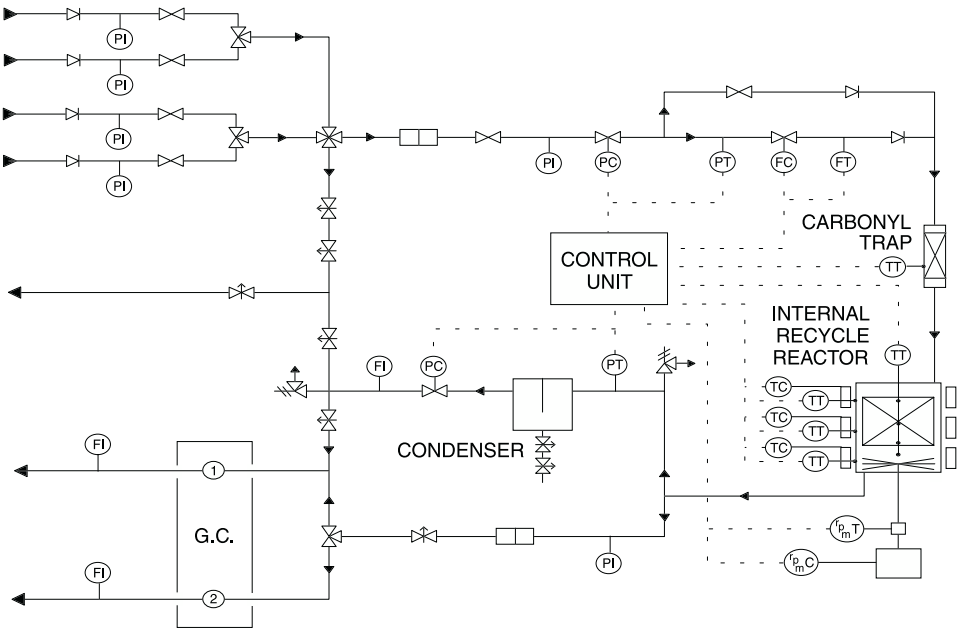

Figure 1. Internal recycle reactor system.

2.3. Kinetic experiments

The experimental set-up for the kinetic measurements, shown in figure 1, consisted of three sections: the feed section, the reactor section, and the analysis section. In the feed section, synthesis and reduction gases were supplied from premixed gas bottles at high pressures. The flow rate was controlled by a Brooks type 5850 TR mass flow controller. The reactants were fed through a heated alumina bead bed, which served to remove any metal carbonyls present and preheat the reactant stream. These gases were used without further purification.

The reactor section consisted of an internal recycle reactor and magnodrive unit. The reactor was designed for operation up to 10.0 MPa and temperatures up to 623 K. The unit was capable of operation with space velocities in the range 1500–50 000 h^{-1} (STP).

Full computer control allowed for long periods of unattended operation. The reactor was made of gold-lined 316 stainless steel. After investigation of the reactor residence time distribution under actual operating conditions, using step and pulse experiments, 1500 rpm was found to be adequate to ensure good mixing. In the kinetic experiments, 5–10 g of catalyst were used. The catalyst pellets were diluted with inert quartz beads of the same size. The reactor had three separate heating bands to give a better temperature control. The temperature inside the reactor was monitored at four locations: just above the catalyst bed, the center of the catalyst bed, the bottom of the catalyst bed, and just beneath the catalyst bed. In this way, the temperature differences within the catalyst bed could be monitored. Under experimental conditions the temperature difference was not more than 5 K.

In the analysis section the product gas stream was split. One stream went to an on-line analysis unit through a bleed line, and the other was fed to a high-pressure, water-cooled condenser where the liquid products were collected and further analyzed. The on-line product analysis line was heated to a minimum of approximately 453 K in order to avoid premature condensation. Condensed products were stored for later detailed analysis. The reactor pressure was measured by an electronic pressure transducer and controlled by a Tescom air-actuated back-pressure regulator after the product gas split.

A dual-channel (Perkin Elmer Model 8500) gas chromatograph (GC) was used for the gas analysis. The GC was equipped with a thermal conductivity detector following a 3 m long 1/8-inch diameter Porapack Q 100–120 mesh column, and a flame ionization detector following a 30 m long 1/32-inch diameter SPB-1 of 0.1 μm thickness. The elaborate analysis procedure permitted a major part of the products to be identified so that accurate mass balances of carbon and hydrogen could be obtained. The carrier gas was helium. Nitrogen (10% v/v) was added to the synthesis gas mixture as an internal standard.

3. Results

3.1. Effect of K loading

Promoter concentration was varied from zero to 10% by weight of K_2O added as K_2CO_3. The catalysts were compared under constant conditions of 4.0 MPa, 563 K, H_2/CO feed ratio of 1.96, and space velocity of 3000 h^{-1} (STP). These particular conditions were

Table 4
Changes in the conversion, yields, and carbon selectivities for changing potassium loadings

	K_2O loading (% w/w)			
	0	1	5	10
CO conversion (%)	95	82	47	42
Exit H_2/CO	18.46	7.39	48.91	13.39
Exit CO/CO_2	0.14	0.91	0.27	0.19
Space time yield (μmol g_{cat}^{-1} min^{-1})				
C_1	153.98	43.19	41.10	37.08
$\geq C_2$	12.40	16.22	22.12	11.34
C_1OH	8.67	16.81	10.55	21.09
$\geq C_2OH$	1.87	3.53	3.92	3.02
Aldehydes	0.82	1.07	0.53	0.48
Carbon selectivity [a] (%)				
C_1	75.06	45.87	51.88	44.98
$\geq C_2$	17.69	30.32	27.92	33.44
C_1OH	5.68	18.92	14.58	17.04
$\geq C_2OH$	1.10	3.75	4.95	3.91
Aldehydes	0.47	1.14	0.67	0.63

[a] Cumulative carbon atom selectivity.

chosen in the light of pre-experiments. The steady-state activity measurements were taken after at least 18 h on stream. The catalyst with a 5% K_2O loading produced the highest higher alcohols to methanol ratio and resulted in overall higher alcohol synthesis activity. Similar optimums for K and Cs loadings were observed in Zn/Cr spinel catalysts [17,18]. The overall activity of the promoted catalyst decreased continuously as the K_2O loading increased from 0 to 10% as shown in table 4, along with the changes in the conversion, yields, and carbon selectivities.

3.2. *Effects of CO conversion, CO_2, and temperature*

Experiments showing the effects of CO conversion with the H_2/CO ratio being equal to 2 at 4.0 MPa and 563 K are illustrated in figure 2. Increasing CO conversion clearly favors the formation of methane but not higher hydrocarbons. On the other hand, it disfavors methanol and higher alcohol selectivities. The selectivities to aldehydes were small and detected only at high CO conversions.

Table 5
Changes in the yields and selectivities for changing CO_2/CO ratio in the exit

	Corresponding inlet CO_2 (%)			
	0	1.96	5.99	10
CO_2/CO in exit	0.03	0.17	0.19	0.24
C_1	17.93	28.90	35.69	37.00
$\geq C_2$	26.80	31.65	29.65	26.23
C_1OH	33.49	17.79	15.65	16.18
$\geq C_2OH$	21.78	21.66	17.65	18.62
Space time yield (μmol g_{cat}^{-1} min^{-1})				
C_1	7.80	39.11	39.65	39.65
$\geq C_2$	5.31	19.54	18.25	14.06
C_1OH	14.58	24.07	21.45	17.34
$\geq C_2OH$	4.15	10.57	11.21	9.98

The effects of CO_2 with an inlet ratio of $H_2/(CO + CO_2)$ equal to 1.96 were studied over 5% K_2O-promoted $Co_2O_3/CuO/ZnO/Al_2O_3$ catalyst. Results at a representative 6000 h^{-1} (STP) space velocity are given in table 5. Increasing the CO_2 content from 0 to 10% at the inlet reduced the selectivity for higher alcohols. Molar ratios of CO to H_2 remained relatively unchanged (at around 2) at the exit over the range of conversions studied while the CO_2 mole fraction at the exit increased slightly. Table 5 also shows that methane selectivity doubled while methanol selectivities decreased sharply as the inlet CO_2 concentration was increased from 0 to 10% CO_2.

The 5% K_2O-promoted $Co_2O_3/CuO/ZnO/Al_2O_3$ catalyst was tested at temperatures of 503, 518, 528, 548, 563, and 583 K (at 4.0 MPa and 3000 h^{-1}). Results

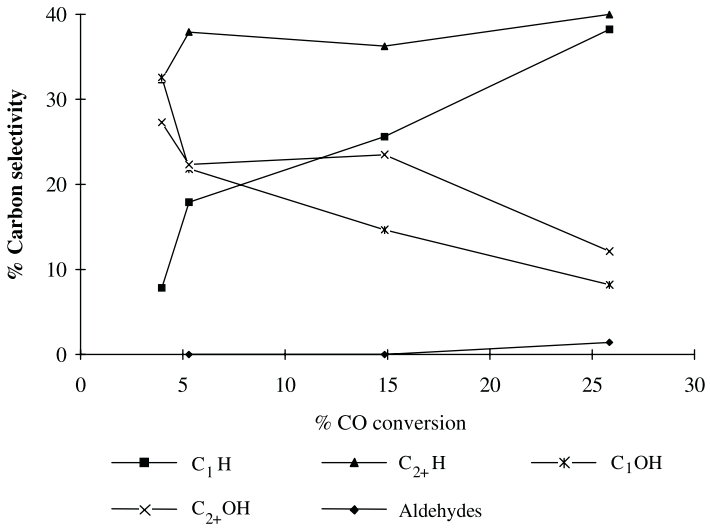

Figure 2. Effects of CO conversion on the selectivity of products.

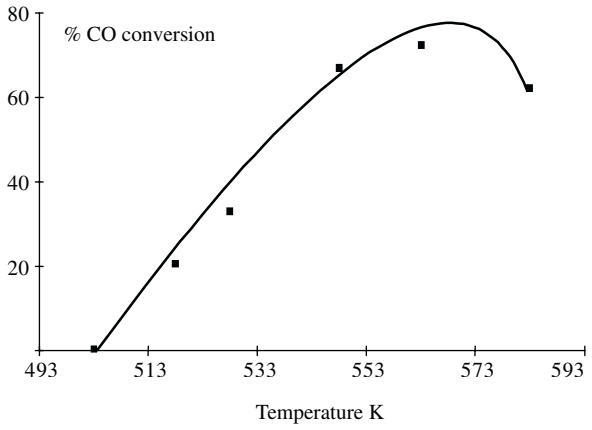

Figure 3. Dependence of CO conversion on temperature.

presented in figure 3 show that CO conversion rates reached at maximum near 563 K. As the temperature was increased there was also a decrease in the average carbon number of alcohols present in the product stream. Changes in the ratio of production rates of higher alcohols to methanol as a function of temperature presented in figure 4 show that, as the temperature increased, the ratio of higher alcohols to methanol increased. Temperatures higher than 563 K caused a decrease in both activity and the ratio of higher alcohols to methanol.

3.3. *XPS characterization of 5% K_2O-promoted Co_2O_3/CuO/ZnO/Al_2O_3 catalyst*

Changes in the Cu $2p_{3/2}$ and Co $2p_{3/2}$ signals are shown, respectively, in figures 5 and 6. Changes in the copper Auger parameters are shown in table 2. Changes in "surface concentrations" of copper and cobalt normalized to zinc are given in table 3.

Prior to treatments, the copper ($2p_{3/2}$) signal in figure 5(a) was clearly due to Cu^{2+} as indicated by the Auger parameter in table 2 and by the characteristic satellite

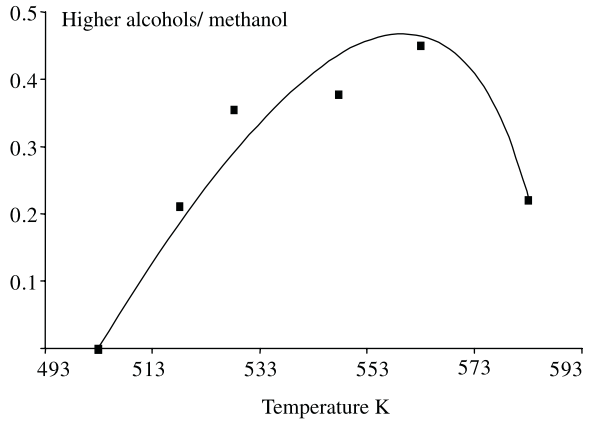

Figure 4. Dependence of the ratio of formation rates of higher alcohols/methanol on operating temperature.

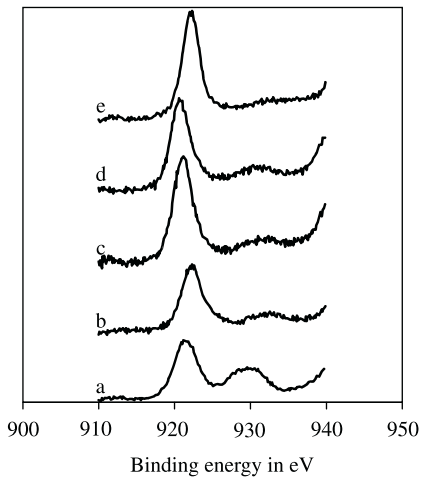

Figure 5. *In situ* XPS Cu $2p_{3/2}$ spectra obtained from a Co_2O_3/CuO/ZnO/Al_2O_3 + 5% K_2O catalyst: (a) 5% K_2O-promoted Co_2O_3/CuO/ZnO/Al_2O_3 higher alcohol synthesis catalyst; (b) after 2 h reduction at 563 K, 0.16 MPa, and with 4.96% H_2 in nitrogen; (c) after 4 h reaction at 563 K, 0.16 MPa, and with 30% CO/10% N_2 in hydrogen; (d) after 10 h reaction at 563 K, 0.16 MPa, and with 30% CO/10% N_2 in hydrogen; (e) after 19 h reaction at 563 K, 0.16 MPa, and with 30% CO/10% N_2 in hydrogen.

peak associated with Cu^{2+}. After 2 h of reduction the catalyst was mostly reduced to Cu^{1+}. Treatment with hydrogen also had the effect of reducing the Cu/Zn ratio from 3.25 to 2.93, as shown in table 3. After reduction, the copper ($2p_{3/2}$) signal becomes narrower, and the satellite structure becomes less evident. Reduction appears to be incomplete, and also indicated by the broader copper and cobalt signals. Analysis of the copper Auger parameters shows that the catalyst turns into a partially oxidized state after the introduction of synthesis gas.

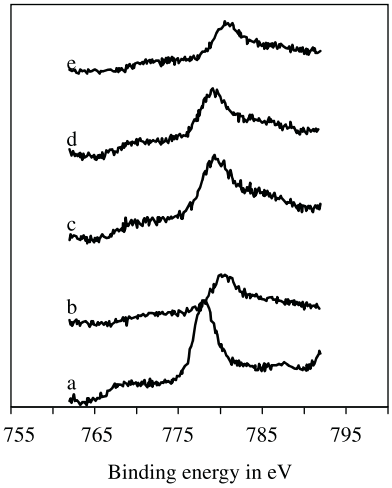

Figure 6. *In situ* XPS Co $2p_{3/2}$ spectra obtained from a Co_2O_3/CuO/ZnO/Al_2O_3 + 5% K_2O catalyst: (a) 5% K_2O-promoted Co_2O_3/CuO/ZnO/Al_2O_3 higher alcohol synthesis catalyst; (b) after 2 h reduction at 563 K, 0.16 MPa, and with 4.96% H_2 in nitrogen; (c) after 4 h reaction at 563 K, 0.16 MPa, and with 30% CO/10% N_2 in hydrogen; (d) after 10 h reaction at 563 K, 0.16 MPa, and with 30% CO/10% N_2 in hydrogen; (e) after 19 h reaction at 563 K, 0.16 MPa, and with 30% CO/10% N_2 in hydrogen.

The differences in binding energies of Co^{2+} and CO^{3+} species in mixed cobalt oxide compounds were not large enough to allow the complete differentiation of the two species. A change of ~2 eV toward the higher binding energy side in the peak position was observed for the reduced catalysts, and a slightly smaller shift to the higher binding energy side for the synthesis gas-exposed catalysts. No change in the shoulder at lower binding energy after treatments was observed, as shown in figure 6.

4. Discussion

Kinetic data used in this study were collected at near steady-state operating conditions since it was found that, especially in the first 10 h of initial operation, the $Co_2O_3/CuO/ZnO/Al_2O_3$ catalyst showed significant changes in both product distribution and in the surface concentration of active components.

The formation of branched products [4,6] is a characteristic feature of K-modified Cu catalysts under higher alcohol synthesis conditions. The absence of branched products in this work demonstrates the copper component of the catalyst is profoundly modified by cobalt. Indeed, based on the product distribution of Co/Cu catalysts, it can be suggested that the role of copper in these catalysts is to steer the usual cobalt products, linear hydrocarbons, toward linear alcohols. In this respect, Sheffer and co-workers [11,19] proposed that Co was the essential component of Co/Cu catalysts for higher alcohol synthesis.

The effect of K on the product distribution over $Co_2O_3/CuO/ZnO/Al_2O_3$ catalysts involves the interaction of potassium with CO [21,22]. The potassium exists as K^{1+} on the catalyst surface [19] and bonds with the oxygen of the surface-bonded CO. Chemisorption studies of Fischer–Tropsch catalysts revealed enhanced carbon oxides and suppressed hydrogen coverage with the addition of potassium [23]. Another view proposed by Courty *et al*. [10,20] for the enhanced alcohol selectivity and decreased methanation is that alkali addition suppresses alcohol dehydration by suppressing the acidic nature of the catalyst.

The addition of K to the $Co_2O_3/CuO/ZnO/Al_2O_3$ catalyst resulted in much suppressed methanation along with an increase in the selectivity of methanol, higher alcohols, and hydrocarbons in line with previous studies [10,11,19,20]. Courty *et al*. [10] noted that the cobalt was not present entirely as metal after reduction. Metallic Co is considered to be responsible for the dissociative adsorption of CO, and also responsible for the production of methane. Suppression of the hydrogenation activity of Co would allow partially hydrogenated CH_x species to remain for longer periods, and these are involved in the C–C chain formation leading to the production of higher hydrocarbons and alcohols.

In this study, the addition of K to the catalyst resulted in the suppression of overall catalytic activity. This might be explained by the enhanced sintering rate of the catalyst (in particular Co and Cu) by K addition, as shown in table 1.

The XPS results in the present study indicate that a significant proportion of Cu and Co species remained oxidized. On the basis of our experimental results, it can be concluded that the Co/Cu-based catalysts remain in a partially oxidized state under working conditions. Courty *et al*. [10] and Dalmon *et al*. [3] observed that using temperature-programmed reduction experiments potassium inhibited the reduction of Co below 593 K. The reduction temperature used in this study was 583 K. Findings of this study are in line with the findings of Courty *et al*. [10].

After exposing the catalyst to a CO_2-containing feed gas, methanation activity increased while the selectivities of higher hydrocarbons and alcohols were adversely affected. Switching the feed gas back to a CO/H_2 mixture, the catalyst recovered its initial activity and selectivity after approximately 2 h. Therefore, it can be proposed that alcohol formation is inhibited by a reversible preferential adsorption of CO_2, possibly on the potassium-promoted active cobalt/copper sites. CO_2 may affect the catalyst's oxidation state through a redox mechanism. It is noteworthy that higher alcohol and higher hydrocarbon selectivity decrease simultaneously as the CO_2 concentration is increased.

Selectivity for higher alcohols can be enhanced by using lower space velocities than those used for methanol synthesis. This can be interpreted as an indication that higher alcohol formation is slow in comparison to the methanol synthesis and occurs subsequent to methanol synthesis [24].

It was found in this study that increasing the CO/H_2 ratio did not considerably increase higher alcohol selectivity. Therefore, it can be tentatively suggested that the reaction of hydroxycarbene and carbene species forming higher alcohol precursors, not the CO insertion [25], was the major chain-growth step. The product distribution suggests that the attachment of CH_x species occurs from the last carbon so that no branched alcohols and hydrocarbons were observed.

With regard to product distributions patterns, Pan *et al*. [25] found a chain propagation factor of 0.71 for higher alcohols. They found that the rate of methanol formation was in line with higher alcohols according to the Schulz–Flory distribution. This was not expected from a chain-growth mechanism in which all the alcohols were produced by CO insertion because the insertion of CO into C_1 species should produce minimum two-carbon-containing products and higher. Therefore, the production of methanol was usually suggested to be occurring at a different active site from the higher alcohol synthesis sites. If there were separate copper sites, producing mainly methanol upon addition of potassium promoter, these promoted

copper catalysts should also have produced some branched alcohols [6,28]. Since there were no branched alcohols in the product distribution, the presence of isolated potassium-promoted copper sites seems unlikely.

It was also reported [10] that higher alcohols and hydrocarbons had the same chain growth probability factor α. In another study, the higher alcohols and higher hydrocarbons had different α [11]. Given that both research groups used similar catalysts, namely Co/Cu-containing catalysts, this was a discrepancy that could not be explained with the existing models of higher alcohol synthesis based on a single site producing different species, namely hydrocarbons and alcohols [26–28].

The calculated chain growth probability factor from the study of Baker *et al.* [14] was found to be 0.36 for alcohols, which is quite similar to the calculated value ($\alpha = 0.35 \pm 0.05$ for alcohols) in this study. On the other hand, hydrocarbons had two different chain growth probability factors: 0.67 ± 0.09 at CO conversion of 3.97% (low conversions) and 0.36 ± 0.05 at a conversion of 25.85% (high conversions). Higher alcohols have one constant chain growth factor (0.35 ± 0.05). At high conversions, the chain growth factor for hydrocarbons was practically the same as that for higher alcohols, as shown in figure 7. Interestingly the rate of methanol formation also falls on the Schulz–Flory line used in chain growth probability factor calculations. This fact can be taken as further indirect evidence that there is only one mechanism through which methanol and higher alcohols are produced.

The chain growth probability factors for higher hydrocarbons vary as CO conversion changes. The change in the calculated chain growth probability factor may be attributed to changes in the oxidation state of the catalysts as the conversion of CO increased.

At high CO conversions both hydrocarbons and alcohols have the same (or converged to the same) chain growth probability factors of 0.36 ± 0.05. At differing CO conversions (from 3 to 25% CO conversion), alcohols had an almost constant chain growth probability factor ($\alpha = 0.35 \pm 0.05$). It can therefore be concluded that there are two different types of active sites for the formation of hydrocarbons or one site changing its characteristics depending on conversion, whereas there is only one type of active site for the formation of alcohols.

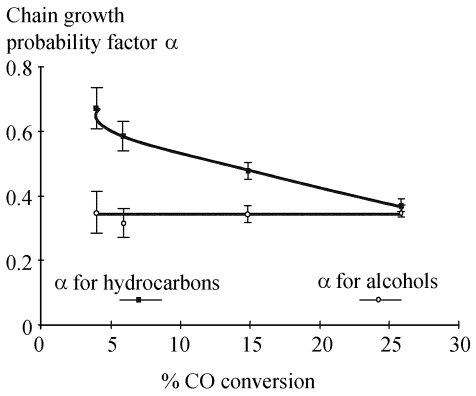

Figure 7. Changes in chain growth probability factor α with CO conversion over a $Co_2O_3/CuO/ZnO/Al_2O_3 + 5\%\ K_2O$ catalyst.

Increasing the CO conversion resulted in an increased CO_2 concentration at the exit. Therefore, the changes in product distributions as the conversion of CO increased may be in part explained by modified active sites responsible for the production of the hydrocarbons with the 0.67 ± 0.09 chain growth probability factor. CO_2 may have modified these active sites by way of reversible competitive adsorption because, when the catalyst operating conditions reverted to low CO conversions, the catalyst regains its selectivity to hydrocarbons with a recovered 0.67 ± 0.09 chain growth probability factor. The kinetic data obtained from the experiments performed on changing CO conversions showed that increasing conversions resulted in increasing hydrocarbon selectivity and simultaneously decreasing alcohol selectivity. At higher conversions, sites producing hydrocarbons having a chain growth probability factor of 0.67 are possibly inhibited by the increased amounts of CO_2 present at high conversions. Moreover, at high CO conversions the alcohols and hydrocarbons had the same chain growth probability factors. These two observations indicate that the hydrocarbons and alcohols are either coming from the same active sites or less possibly hydrocarbons are emanating from alcohols.

5. Conclusions

In modifying a methanol synthesis catalyst by the addition of Co and K for use in higher alcohol synthesis, K-promoted Co/Cu-based catalysts are moderately selective for production of higher alcohols under mild conditions. The highest selectivity is obtained from a 5% K_2O promoter concentration. It is found that there is a clear maximum temperature for higher alcohol selectivity and yield. At low conversions, there are two different active sites with two distinctly different chain growth probability factors. At high conversions, there is only one type of active site producing alcohols and hydrocarbons with the same chain growth probability factor.

Acknowledgment

This work was supported by the State Planning Agency of Turkey, project number 97K121720.

References

[1] X. Xiaoding, E.B.M. Doesburg and J.J.F. Scholten, Catal. Today 2 (1987) 125.

[2] P. Forzatti, E. Tronconi and I. Pasquon, Catal. Rev. Sci. Eng. 33 (1991) 109.
[3] J.A. Dalmon, P. Chaumette and C. Mirodatos, Catal. Today 15 (1992) 101.
[4] K.J. Smith and R.B. Anderson, J. Catal. 85 (1984) 428.
[5] J.M. Campos-Martin, A. Guerrero-Ruiz and L.G. Fierro, J. Catal. 156 (1995) 208.
[6] I. Boz, M. Sahibzada and I.S. Metcalfe, Ind. Eng. Chem. Res. 33 (1994) 2021.
[7] M. Ichikawa, T. Fukushima and K. Shikakura, Proc. 8th Int. Cong. Catal., West Berlin, 1984, p. 69.
[8] H. Arakawa, T. Hanaoka, T. Takeuchi, T. Matsuzaki and Y. Sugi, Proc. 9th Int. Cong. Catal., Calgary, 1988, p. 610.
[9] A. Sugier and E. Freund, US Patent 4 122 110 (1978).
[10] Ph. Courty, D. Durand, E. Freund and A. Sugier, J. Mol. Catal. 17 (1982) 241.
[11] G.R. Sheffer, R.A. Jacobson and T.S. King, J. Catal. 116 (1989) 95.
[12] M. Blanchard, H. Derule and P. Canesson, Catal. Lett. 2 (1989) 319.
[13] J.M. Berty, Chem. Eng. Prog. 70 (1974) 78.
[14] J.E. Baker, R. Burch and S.E. Golunski, Appl. Catal. 53 (1989) 279.
[15] D. Briggs and M.P. Seah, *Practical Surface Analysis* (Wiley, 1983).
[16] G. Moretti, M. Fierro, M.Lo. Jacono and P. Porta, Surf. Interf. Anal. 14 (1989) 325.
[17] W.S. Epling, G.B. Hoflund, W.M. Hart and D.M. Minahan, J. Catal. 169 (1997) 438.
[18] W.S. Epling, G.B. Hoflund, W.M. Hart and D.M. Minahan, J. Catal. 172 (1997) 13.
[19] G.R. Sheffer and T.S. King, Appl. Catal. 44 (1988) 153.
[20] Ph. Courty, J.P. Airle, A. Convers, P. Mikitenko and A. Sugier, Hydrocarbon Process. 34-A (1985).
[21] R.M. Bailliard-Letournel, A.J.G. Cobo, C. Mirodatos, M. Primet and J.A. Dalmon, Catal. Lett. 2 (1989) 149.
[22] N. Mouaddib and V. Perrichon, Proc. 9th Int. Cong. Catal., Calgary, 1988, p. 521.
[23] M.E. Dry and G.J. Oosthuizen, J. Catal. 11 (1968) 18.
[24] E. Tronconi, F. Ferlazzo, P. Forzatti and I. Pasquon, Ind. Eng. Chem. Res. 26 (1987) 2122.
[25] W.X. Pan, R. Cao and G.L. Griffin, J. Catal. 114 (1988) 447.
[26] A. Kiennemann, H. Idriss, R. Kieffer, P. Chaumette and D. Durand, Ind. Eng. Chem. Res. 30 (1991) 1130.
[27] W.X. Pan, R. Cao and G.L. Griffin, Langmuir 4 (1988) 1108.
[28] K.J. Smith and R.B. Anderson, Can. J. Chem. Eng. 61 (1983) 40.